Early termination of the Shiga toxin transcript generates a regulatory small RNA

Brandon M. Sy[a], Ruiting Lan[a], and Jai J. Tree[a,1]

[a]School of Biotechnology and Biomolecular Sciences, University of New South Wales, Sydney, NSW 2052, Australia

Edited by Gisela Storz, National Institute of Child Health and Human Development, Bethesda, MD, and approved August 28, 2020 (received for review April 9, 2020)

Enterohemorrhagic *Escherichia coli* is a significant human pathogen that causes disease ranging from hemorrhagic colitis to hemolytic uremic syndrome. The latter can lead to potentially fatal renal failure and is caused by the release of Shiga toxins that are encoded within lambdoid bacteriophages. The toxins are encoded within the late transcript of the phage and are regulated by antitermination of the $P_{R'}$ late promoter during lytic induction of the phage. During lysogeny, the late transcript is prematurely terminated at $t_{R'}$ immediately downstream of $P_{R'}$, generating a short RNA that is a byproduct of antitermination regulation. We demonstrate that this short transcript binds the small RNA chaperone Hfq, and is processed into a stable 74-nt regulatory small RNA that we have termed StxS. StxS represses expression of Shiga toxin 1 under lysogenic conditions through direct interactions with the *stx1AB* transcript. StxS acts *in trans* to activate expression of the general stress response sigma factor, RpoS, through direct interactions with an activating seed sequence within the 5′ UTR. Activation of RpoS promotes high cell density growth under nutrient-limiting conditions. Many phages utilize antitermination to regulate the lytic/lysogenic switch and our results demonstrate that short RNAs generated as a byproduct of this regulation can acquire regulatory small RNA functions that modulate host fitness.

sRNA | lambda phage | Shiga toxin | ncRNA | noncoding RNA

Many bacterial pathogens have horizontally acquired exotoxins through bacteriophages that confer severe disease phenotypes. These include *Staphylococcus aureus*, *Streptococcus spp.*, *Vibrio cholera*, *Clostridium botulinum*, *Corynebacterium diptheriae*, and a broad pathotype of *Escherichia coli* termed enterohemorrhagic *E. coli* (EHEC) that are partly characterized by the acquisition of Shiga toxin genes within lambdoid bacteriophages (1, 2). Shiga toxins (Stx) are AB5-family toxins that are endocytosed by Gb3-expressing renal endothelial cells in the kidneys (3). The StxA subunit is released within the cell cytoplasm and causes cell death by depurinating ribosomal 28S RNA, leading to tissue destruction and potentially progressing to fatal thrombocytopenia, hemolytic anemia, and renal failure, a triad of sequelae that are collectively termed hemolytic uremic syndrome (HUS) (4). Severe disease symptoms are commonly associated with *E. coli* serotype O157:H7, although non-O157:H7 serotypes are increasingly reported to cause HUS (5, 6).

Shiga toxins are integrated into the late region of the Stx phage and are transcribed from the phage late promoter $P_{R'}$ during lytic induction of the bacteriophage (7–9). Lambdoid bacteriophages are regulated by antitermination whereby the early and late promoters, P_L, P_R, and $P_{R'}$, are terminated at downstream intrinsic terminators, t_L, t_R, and $t_{R'}$, respectively (10). Lytic development of the phage is induced by the RecA-mediated SOS response and both DNA damaging agents and select antibiotics are known to promote phage lytic induction and toxin production. RecA-mediated induction relieves P_L and P_R repression and leads to a cascade of regulatory events that culminate in expression of the antiterminators N and Q that modify RNA polymerase and prevent termination at t_L, t_R, and $t_{R'}$. Antitermination of the late $P_{R'}$ transcript at $t_{R'}$ allows transcription of the late genes that include the Shiga toxin and lysis genes (7). The toxin is released from the host cell by phage-induced lysis and during RecA-mediated induction the amount of toxin produced is a function of the lytic induction frequency of the phage. Notably, the Stx1 toxin is also regulated from an independent promoter termed P_{stx1} that is repressed by the iron-responsive transcription factor, Fur, in response to iron sufficiency and nitric oxide (8, 11, 12). Transcription from P_{stx1} leads to Stx1 expression and release in the absence of phage-induced lysis or phage particle production.

During lysogeny, the Stxϕ late promoter $P_{R'}$ is constitutively active, but constitutively terminated at $t_{R'}$ generating a short transcript as a byproduct of regulation by antitermination. We had previously reported that this region interacts with the small RNA chaperone Hfq (13), and here we demonstrate that the transcript is processed by the major endoribonuclease RNase E into a stable 74-nt *trans*-acting regulatory small RNA (sRNA) that we term the Shiga toxin small RNA, StxS. We demonstrate that StxS activates the stationary phase general stress response sigma factor *rpoS* by commandeering an activating seed region within the 5′ UTR that is utilized by host-encoded regulatory sRNAs. StxS activation of RpoS allows EHEC to reach a higher cell density in stationary phase growth. StxS also represses expression of Shiga toxin 1 under lysogenic conditions through direct interactions with the *stx1B* ribosomal binding site.

Results

The Shiga Toxin Bacteriophages of Enterohemorrhagic *E. coli* O157:H7 Encode Hfq-Binding Small RNAs. During our earlier analysis of Hfq-binding sites within the EHEC O157:H7 str. Sakai transcriptome

Significance

Enterohemorrhagic *E. coli* is a significant human pathogen that can cause severe disease due to the release of Shiga toxins. The toxins are encoded within lysogenic bacteriophage and controlled by antitermination of the phage late promoter, $P_{R'}$. This promoter is always active, but terminated immediately downstream during lysogeny. A byproduct of antitermination regulation is transcription of a short RNA that is thought to be nonfunctional. Here we demonstrate that in Shiga toxin-encoding phages, this short RNA is a Hfq-binding regulatory small RNA. The small RNA represses toxin production threefold under lysogenic conditions and promotes high cell density growth. Lysogenic bacteriophages are highly abundant and our results suggest that antiterminated phage promoters may be a rich source of regulatory RNAs.

Author contributions: B.M.S. and J.J.T. designed research; B.M.S. performed research; R.L. contributed new reagents/analytic tools; B.M.S., R.L., and J.J.T. analyzed data; and B.M.S. and J.J.T. wrote the paper.

The authors declare no competing interest.

This article is a PNAS Direct Submission.

[1]To whom correspondence may be addressed. Email: j.tree@unsw.edu.au.

This article contains supporting information online at https://www.pnas.org/lookup/suppl/doi:10.1073/pnas.2006730117/-/DCSupplemental.

First published September 23, 2020.

we identified 11 orphan Hfq-binding sites in the Stx1 and Stx2a encoding phages (Stx1ϕ and Stx2aϕ, also termed Sp15 and Sp5, respectively), defined as Hfq-binding peaks >100 nucleotides from a genomic feature and present in more than two replicate experiments. Northern blot analysis of a subset of predicted Stxϕ-encoded sRNAs confirmed that six produced short RNA fragments (13). The Stx1AB genes of the cryptic Stx1ϕ are "bookended" by the sRNA EcOnc42 3′ of the toxin, and a putative sRNA termed EcOnc15 within the 5′ region of the toxin transcript (*SI Appendix*, Fig. S1). EcOnc15 is positioned between the late phage promoter $P_{R'}$ that drives Stx1AB transcription and the constitutive terminator $t_{R'}$, that prematurely terminates transcription of *stx1AB* during lysogeny (7, 8). A Hfq-binding site was identified at the same position within the Stx2aϕ (Sp5) but was omitted from our predicted sRNAs because of the proximity of a downstream ORF (*SI Appendix*, Fig. S2). Deletions within Hfq CRAC sequencing reads, that indicate sites of direct protein–RNA contact, were also recovered within StxS, indicating direct Hfq contact (see Fig. 2*A*). The Stx1ϕ and Stx2aϕ $P_{R'}$ terminated transcripts are highly homologous, and share 94% sequence identity (*SI Appendix*, Fig. S3). The predicted size for the $t_{R'}$ terminated $P_{R'}$ transcript is 258 nt, however a shorter 74-nt transcript was detected by Northern blot analysis, suggesting that the Stx1ϕ and Stx2aϕ copies of EcOnc15 are processed by a ribonuclease or transcribed from an internal promoter (Fig. 1 *A* and *B*). Analysis of EHEC cultures grown in minimal and rich media indicated the short $P_{R'}$ transcript accumulated in early stationary phase cultures when grown in rich (Luria-Bertani media, [LB]) or minimal media (M9) (Fig. 1*B*). EcOnc15 was highly expressed in all growth stages in virulence-inducing MEM-HEPES media (type 3 secretion inducing). EcOnc15 is encoded within the 5′ region of the antiterminated *stxAB* mRNA (Fig. 1*A*) and we have termed this prematurely terminated, Hfq-binding small RNA the Shiga toxin small RNA, StxS.

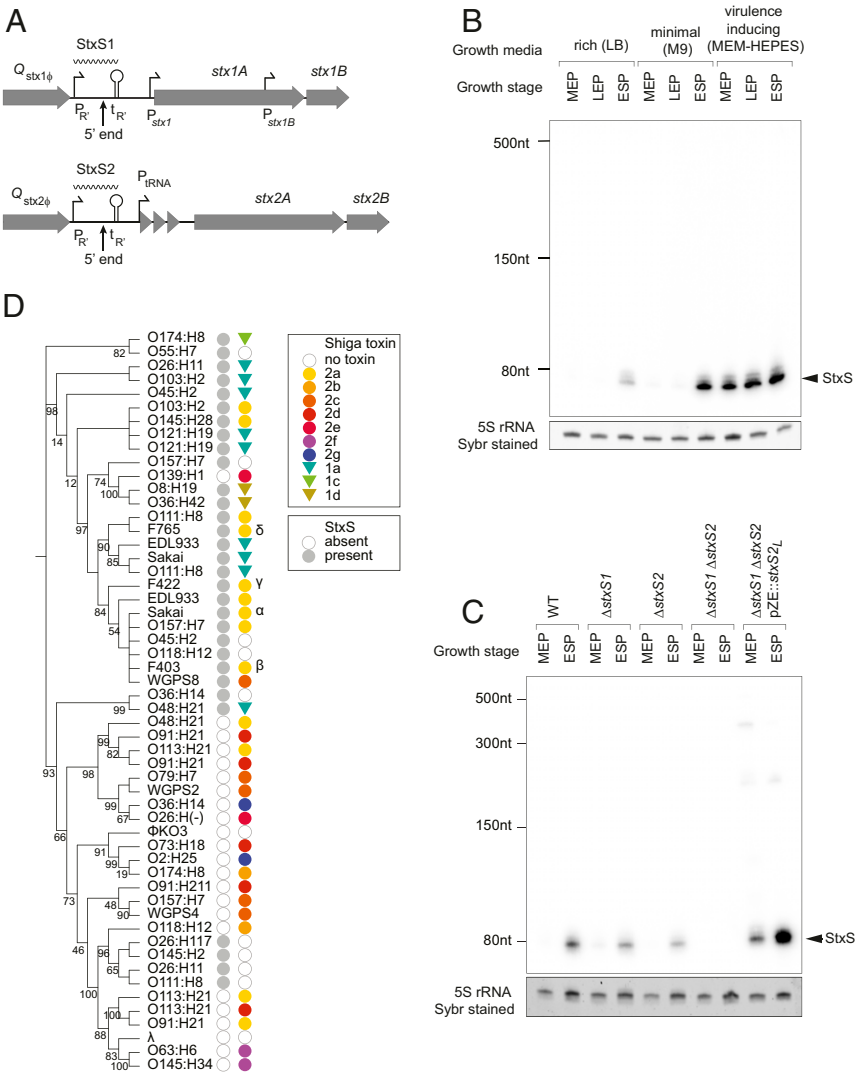

Fig. 1. Shiga toxin-encoding phages transcribe a small, Hfq-binding RNA from the late phage promoter $P_{R'}$. (*A*) Genetic organization of the *stx1AB* (*Top*) and *stx2AB (Bottom)* loci. Promoters are indicated as bent arrows and intrinsic terminators as hairpins. Annotated gene features are indicated as gray arrows. Full-length StxS is indicated as a wavy line and the abundant 5′ end is indicated below (black arrow). (*B*) Northern blot analysis of StxS expression in rich, minimal, and virulence-inducing media (indicated above) and at midexponential growth phase (MEP, OD_{600} 0.6), late exponential phase (LEP, OD_{600} 1.0), and early stationary phase (ESP, OD_{600} 2.0). Sybr Safe staining of 5S rRNA is shown below and migration of StxS is indicated by a black arrow. (*C*) Northern blot analysis of StxS expression in minimal M9 media at MEP and ESP from EHEC str. Sakai and isogenic mutants (indicated above). (*D*) Maximum-likelihood phylogenetic tree showing relationships of Q antiterminator proteins from representative Shiga-toxigenic phages (serotype or strain indicated). The presence (gray-shaded circle) or absence (unshaded circle) of StxS sequence downstream of Q is indicated, and the Shiga toxin 1 (colored triangles) or Shiga toxin 2 (colored circles) subclasses are indicated in the *Right* columns.

Stx1ϕ and Stx2ϕ Express StxS Small RNA. To determine whether both copies of the Stx phage in EHEC O157:H7 strain Sakai transcribe StxS sRNA, single deletions of *stxS1* (EcOnc15 encoded within the Stx1ϕ) and *stxS2* (encoded within the Stx2aϕ), and a double deletion of both *stxS1* and *stxS2* were constructed in a toxin inactivated derivative of strain Sakai (14). The short StxS transcript (74 nt, here termed $StxS_S$) was detected in both single deletion strains but not in the double deletion, indicating that both Stx phages produce the $StxS_S$ transcript (Fig. 1*C*). The double deletion was complemented with a plasmid transcribing the full-length StxS (here termed $StxS_L$) from a constitutive promoter ($P_{LlacO-1}$) and restored expression that was higher in midexponential and early stationary phase (Fig. 1*C*). These results indicate that both copies of StxS are transcribed and produce roughly equivalent amounts of the short 74-nt $StxS_S$ RNA that accumulates in early stationary phase cultures.

We next looked at StxS sequence conservation between diverse Stxϕ. StxS is encoded directly downstream of the Q antiterminator and the presence of StxS was correlated with Q phylogeny, consistent with the close association of these alleles (Fig. 1*D*). Q protein sequences from Stx-encoding phage clustered into two major clades reflecting a 144- and 207-amino acid Q protein. The shorter Q was correlated with the presence of StxS, and the sRNA is predominantly encoded 5′ of Stx1 and Stx2a toxins (Fig. 1*D*). StxS was found in Stx2a subclasses α to γ that produce variable amounts of toxin (15), suggesting that StxS is not responsible for the variability observed between these classes. Interestingly, several nontoxigenic phages also encoded StxS, including atypical enteropathogenic *E. coli* serotype O55:H7 that is proposed to be a progenitor of the EHEC1 lineage. Collectively, these results demonstrate that StxS is predominantly encoded within Stx1 and Stx2a phages that have been linked with more severe human disease, and both Stx-encoding phages of EHEC O157:H7 str. Sakai express StxS that accumulates in stationary phase cultures.

RNase E Processing Generates a Stable 3′ Small RNA. The $P_{R'}$ to $t_{R'}$ region of the Stx1ϕ and Stx2aϕ is 258 nt, suggesting StxS is processed by ribonucleases or transcribed from an internal promoter. Using differential RNA sequencing (dRNA-seq) we mapped both triphosphorylated and monophosphorylated RNA 5′ ends throughout the transcriptome. Primary transcription start sites and processed RNA 5′ ends were identified throughout the lysogenic phages and within the lytic subpopulation of the culture using TSSPredator version 1.06 (16). We were able to identify the antiterminated promoters P_L, P_R, and $P_{R'}$, the early lysogenic promoters P_I and P_{RE}, and the promoter for maintenance of lysogeny, P_{RM} (*SI Appendix*, Figs. S1 and S2 and Dataset S1). dRNA-seq analysis identified the primary transcription start site of the late promoter $P_{R'}$ positioned at 1,266,203 in the Stx2aϕ and 2,926,201 in the Stx1ϕ, 258 nt from $t_{R'}$ and consistent with earlier work demonstrating that *stxAB* is transcribed from a promoter closely associated with *Q* (7, 8) (Dataset S1). Notably, we were not able to detect the P_{stx1} promoter upstream of *stx1AB*, likely due to the deletion of a 600-nt BsiWi fragment in the toxin-attenuated strain which covers the region upstream of the Stx1 coding sequence (14). Two additional primary transcription start sites were called upstream of *stx2AB*, the first mapping to a promoter between $t_{R'}$ and *stx2AB* that appears to drive transcription of the downstream tRNAs, and a transcription start site at the 5′ end of $StxS_S$ (Fig. 2*A* and *SI Appendix*, Fig. S2). We next used Term-seq to map the position of RNA 3′ ends within the Stxϕ and identify the precise position of the StxS 3′ end ($t_{R'}$) (17). The 3′ end of StxS was mapped to 258 nt downstream of $P_{R'}$ in both the Stx2aϕ and Stx1ϕ (1,266,460 and 2,925,944, respectively), consistent with the position of the predicted $t_{R'}$ intrinsic terminator (Fig. 2*A*).

To determine if the 5′ end of $StxS_S$ is generated by processing or an independent promoter, we used RNA linker-mediated rapid amplification of cDNA ends (RLM-RACE) to map the 5′ end of the 74-nt fragment in the presence or absence of tobacco acid pyrophosphatase (TAP, Fig. 2*B*). The 5′ end of the short $StxS_S$ fragment was readily detected by RLM-RACE in the absence of TAP, suggesting that the $StxS_S$ transcript is generated by ribonuclease processing of the 258-nt $StxS_L$ RNA that is transcribed from the late promoter, $P_{R'}$. RNase E is the major endoribonuclease in *E. coli* and we next analyzed published RNase E UV cross-linking data to determine if RNase E bound the 5′ end of the short $StxS_S$ fragment (18). RNase E cross-linked to both StxS1 and StxS2 with reads peaking within both the 3′ 74 nt and 5′ region (Fig. 2*A*). Deletions within sequencing reads derived from cross-linking were also recovered within StxS, indicating direct RNase E contact (Fig. 2*A*). RNase E cleaves single-stranded RNA at RN↓WUU motifs (19). RNase E contact-dependent deletions flanked a GUAUU site and were maximal at positions −62 nt, and +40/+65 nt from the cleavage site (Fig. 2*A*). Cleavage within the RNase E motif at GU↓AUU was consistent with the $StxS_S$ 5′ end identified by dRNA-seq, and 8 nt upstream of the 5′ end recovered by RLM-RACE. These results indicate that RNase E contacts $StxS_L$ and cleaves within an RNase E motif at position +173 to release $StxS_S$.

To verify that RNase E is required for processing, $StxS_L$ was cloned into pBR322 with the native $P_{R'}$ promoter and accumulation monitored in an *E. coli* strain producing the temperature sensitive RNase E allele, *rne-3071*. Shifting the $StxS_L$ transcribing culture to the nonpermissive temperature (44 °C) for 30 min led to a marked increase in $StxS_L$ (Fig. 2*C*). These results strongly support RNase E processing of $StxS_L$ within the GU↓AUU motif at position +173 nt to generate a stable 74 nt 3′ $StxS_S$ small RNA.

StxS Is Not Required for Propagation of Shiga-Toxigenic Bacteriophage. Lambdoid bacteriophage express regulatory RNAs that control the lytic-lysogenic switch including OOP and paQ transcripts (20, 21). To determine if StxS plays a role in the lytic-lysogenic switch, we constructed single and double StxS deletions using allelic exchange in the wild type (WT), toxigenic EHEC O157:H7 str. Sakai that does not have insertions or deletions within the *stxAB* genes. Deletions were constructed so that $P_{R'}$, the predicted Q utilization site (*qut*), and $t_{R'}$ remained within the phage (*SI Appendix*, Fig. S4*A*). We additionally repaired the chromosomal deletion of each *stxS* copy using CRISPR-Cas9 to assay complementation of any phage propagation defect. As CRISPR-Cas9 induces DNA damage that may trigger excision of prophages, we used whole genome sequencing to confirm that no secondary mutations or loss of prophage had occurred during construction of the deletion and complementation strains (*SI Appendix*, Table S1). Filtered, phage-containing supernatants were prepared after mitomycin C induction and phage particles enumerated using a spot dilution assay (*SI Appendix*, Fig. S4*B*) (22, 23). We were not able to detect a significant change in plaquing in the single, double, or repaired *stxS* mutants. These results indicate that StxS is not required for propagation of the Stx2ϕ and that the StxS sRNA may have been co-opted for functions outside of bacteriophage regulation.

StxS Activates RpoS Expression Using the Same Seed Region as Core Genome-Encoded sRNAs. Our results indicated that StxS does not act *in cis* during Stxϕ propagation, and suggested that StxS may function as a *trans*-acting regulatory sRNA. To identify mRNA targets that form base-pairing interactions with StxS, we extracted all RNA–RNA interactions that mapped within the coordinates for StxS1 and StxS2 from our earlier RNase E-CLASH sRNA interactome dataset (18) (*SI Appendix*, Table S2). Statistically significant RNA interactions that were represented by more than one hybrid read were recovered for 11 target RNAs, including the stationary phase general stress response sigma factor *rpoS*, *adhE*, *mobA*, *rmf*, and the type 3 secreted effector *nleD*. UNAfold hybrid-min (24) was used to predict base-pairing interactions between StxS and mRNA hybrid sequences. Base-pairing interactions were identified within

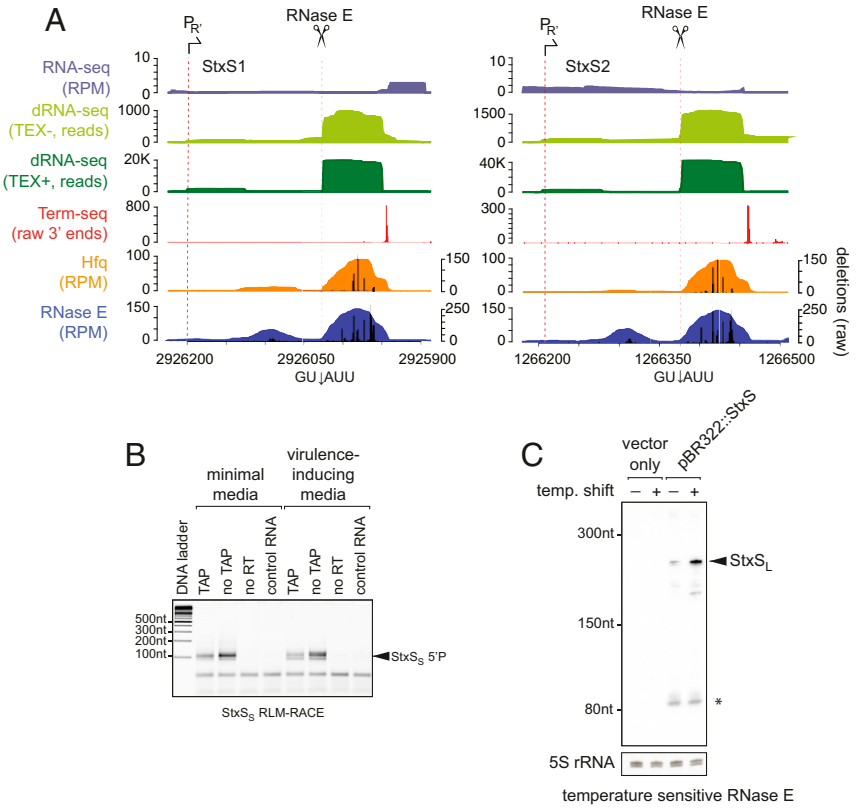

Fig. 2. StxS small RNA is processed by the endoribonuclease RNase E. (*A*) RNA sequencing data mapping to StxS1 (Stx1ϕ, *Left*) and StxS2 (Stx2ϕ, *Right*). From *Top* to *Bottom*, total RNA-sequencing data (reads per million, RPM) (dark blue), dRNA-seq (raw read count) data with (dark green) or without (light green) TEX treatment, Term-seq RNA 3′ ends (red, raw read count), and Hfq- (orange) and RNase E-binding sites (dark blue) from UV cross-linking and sequencing datasets (BioProjects PRJNA197291 and PRJNA310426), respectively. Sequencing deletions (raw read count) indicating points of direct contact with Hfq and RNase E are overlaid as a barplot (black, *Right y* axis). The phage late promoter $P_{R'}$ and RNase E cleavage sites are indicated above. The position of the RNase E recognition motif is indicated below the plot. The *x* axis represents the genomic coordinates spanning the StxS alleles. (*B*) RLM-RACE analysis of the 5′ end of the 74-nt StxS fragment, $StxS_S$. Total RNA for RLM-RACE was extracted from EHEC str. Sakai grown in minimal (M9) media or virulence-inducing media (supplemented MEM-HEPES). RLM-RACE was performed with or without TAP (indicated above). (*C*) RNase E processes the longer 258-nt StxS transcript, $StxS_L$. Northern blot analysis of heterologously expressed $StxS_L$ in a temperature-sensitive RNase E (*rne-3071*) background. Cultures were shifted to permissive or nonpermissive temperature (indicated above) for 30 min before harvesting total RNA. Migration of $StxS_L$ is indicated by the black arrow. An asterisk indicates a band of nonspecific hybridization or a $StxS_L$ degradation product.

$StxS_S$, consistent with the processed 3′ fragment containing the functional portion of the transcript (Fig. 3*A*). StxS interactions with *rpoS* were 10-fold higher than any other mRNA (113 unique hybrids, *SI Appendix*, Table S2), suggesting that a major function of StxS is regulation of the stationary phase stress response sigma factor. Notably, $StxS_S$ base pairs with the previously identified *rpoS* seed sequence used by the sRNAs RprA, DsrA, and ArcZ that activate expression of *rpoS* mRNA (Fig. 3*B*) (25–28).

To confirm that StxS regulates *rpoS* expression by direct base-paring interactions we constructed a translational sfGFP fusion to the *rpoS* 5′ UTR and 30-nt of the CDS under the control of the constitutive promoter $P_{LletO\text{-}1}$. RpoS′-sfGFP fluorescence was monitored in *E. coli* DH5α in the presence or absence of $StxS_L$ cloned under the control of the constitutive promoter $P_{LlacO\text{-}1}$. In the presence of StxS, fluorescence increased 5.3-fold above the plasmid only control, indicating that StxS strongly activates RpoS expression (Fig. 3*C*). To confirm that StxS directly base pairs with the *rpoS* 5′ UTR, compensatory point mutations were introduced into the StxS and *rpoS* seed regions (Fig. 3*B*). Mutation of either the StxS or *rpoS* seed abolished activation of *rpoS*′-sfGFP expression (Fig. 3*C*). When compensatory mutations were both provided, activation of *rpoS*′-sfGFP translation was restored, confirming that StxS directly activates translation of *rpoS* by base pairing with an activating seed region (Fig. 3*C*). To confirm our results we used an electrophoretic mobility shift assay (EMSA) to characterize the StxS-*rpoS* interaction in vitro. Addition of StxS to radiolabeled *rpoS* 5′ UTR shifted the radiolabeled complex to a slower migrating species consistent with duplex formation between StxS and *rpoS* (Fig. 3*D*)

Recent work has demonstrated that activation of *rpoS* by RprA, DsrA, and ArcZ act in part through inhibition of premature Rho termination (29). To understand if StxS also acts through Rho-dependent and -independent pathways we looked at StxS activation in the presence or absence of the Rho inhibitor, bicyclomycin (BCM). Addition of bicyclomycin significantly increased expression of the RpoS′-sfGFP fusion 1 h postinduction, consistent with premature termination of this transcript (*SI Appendix*, Fig. S5*A*). StxS was able to further activate expression of the RpoS′-sfGFP fusion in the presence of bicyclomycin at 45 and 60 min postinduction, and the increase in expression with both BCM and StxS was additive. These results indicate that StxS is able to activate *rpoS* through a Rho-independent mechanism, likely through unfolding of the inhibitory secondary structure within the 5′ UTR (25, 30). Notably, our full-length RpoS′-GFP translational fusion is subject to both Rho-dependent termination and Rho-independent translation inhibition and our results do not preclude a further Rho-dependent activity.

We next asked whether *rpoS* transcription and translation is activated by StxS in the pathogen, EHEC. A transcriptional fusion containing the native *rpoS* promoter, 5′ UTR, and 31 nucleotides

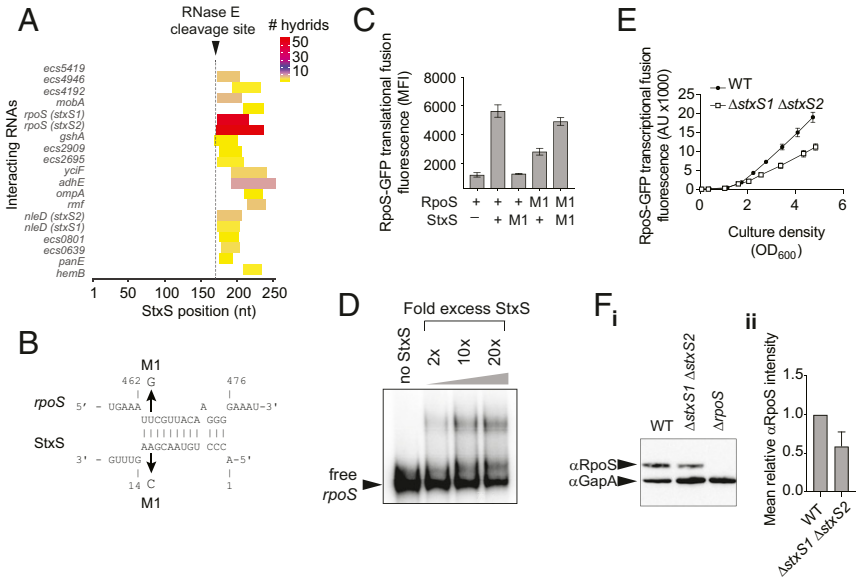

Fig. 3. StxS is a *trans*-acting regulatory small RNA that activates expression of the stationary phase stress response sigma factor, RpoS. (*A*) Statistically significant mRNA interactions (false discovery rate [FDR] ≤0.05 and represented by more than one unique hybrid read) recovered from RNase E-CLASH (18) are presented. Transcript names are indicated (*Left*) and shaded areas indicate the region of StxS ligated to the mRNA and predicted to base pair with the target. Colors indicate the number of unique hybrid reads recovered for each RNA-StxS interaction. The dashed line indicates the position of RNase E cleavage and the 5′ end of $StxS_S$. (*B*) Predicted base pairing between StxS and the *rpoS* 5′ UTR. Positions indicated *Above* and *Below* are relative to the transcript 5′ end. M1 indicates the compensatory nucleotide changes introduced to destabilize base pairing between StxS and *rpoS* mRNA. (*C*) Fluorescence of a constitutively transcribed RpoS′-sfGFP translational fusion was assessed in the presence or absence of StxS (indicated below). Constructs containing compensatory M1 mutations (presented in *B*) are also indicated. Fluorescence represents the median fluorescence intensity (MFI) of biological triplicate cultures. Error bars represent SD. (*D*) EMSA analysis of the StxS-*rpoS* interaction. A radiolabeled fragment of the *rpoS* 5′ UTR spanning positions 260 to 576 (~50 fmol) was incubated with a 2-, 10-, or 20-fold excess of unlabeled StxS and separated on a native 6% polyacrylamide gel. Migration of the free *rpoS* RNA is indicated by the arrowhead. The *Upper* bands represent a slower migrating StxS-*stx1B* complex. (*E*) Fluorescence of an RpoS′-eGFP transcriptional fusion during growth in minimal M9 media in EHEC str. Sakai or the isogenic Δ*stxS1* Δ*stxS2* mutant. Fluorescence was measured in arbitrary units (AU) and represents the average of five biological replicates. Error bars represent SD. (*F*, *i*) Western blot analysis of RpoS protein levels in EHEC (WT), Δ*stxS1*, Δ*stxS2*, and Δ*rpoS* deletions. The blot was probed with α-RpoS and α-GapA (loading control) antibodies (indicated by black arrows). (*ii*) Mean normalized α-RpoS signal intensity in the Δ*stxS1* Δ*stxS2* strain measured relative to EHEC (WT) levels. Error bars represent SD from four replicate experiments.

of the CDS was fused to eGFP in the medium copy number vector pAJR70. Fluorescence was monitored in the wild type, non-toxigenic EHEC str. Sakai and Δ*stxS1* Δ*stxS2* backgrounds. Deletion of StxS decreased RpoS′-eGFP expression 41.2% in stationary phase cells (Fig. 3*E*), consistent with earlier results in nonpathogenic *E. coli* (Fig. 3*C*). Similar results were obtained when directly assaying RpoS protein levels using a monoclonal antibody. RpoS was reduced 49% in the Δ*stxS1* Δ*stxS2* background (Fig. 3*F*). A significant decrease in the RpoS-regulated transcripts *osmY* and *katE* was also observed in the double *stxS* mutant (*SI Appendix*, Fig. S5*B*). Collectively these results demonstrate that StxS is a *trans*-acting regulatory sRNA that activates expression of the stationary phase stress sigma factor RpoS and the RpoS-regulon in EHEC.

StxS Promotes Increased Stationary Phase Culture Density in Nutrient-Limiting Conditions. RpoS plays a critical role in adaptation to stationary phase growth conditions and regulates 1,135 genes in EHEC (31). Our results suggested that StxS may increase the stress tolerance of Stx phage lysogens through activation of *rpoS* translation. Stress tolerance was tested in the single and double *stxS* deletion background. Deletion of StxS did not affect resistance to mild, chronic acid stress or acute acid shock (*SI Appendix*, Fig. S6 *A* and *B*). The double deletion had a modest growth defect when grown under osmotic stress conditions (*SI Appendix*, Fig. S6*C*). The Δ*stxS1* Δ*stxS2* mutant grew similar to wild type in rich media, but grew to a lower stationary phase cell density in minimal M9 medium (Fig. 4 *A*, *i* and *ii*). Complementation of the double deletion *in trans* restored stationary phase cell density to wild-type levels (Fig. 4 *A*, *iii*). Viable cell counts were used to directly assess the growth defect under nutrient-limited conditions. The wild-type EHEC strain had 20.2% and 25.4% higher cell counts in stationary phase than the Δ*stxS1* Δ*stxS2* and Δ*rpoS* strains, respectively (Fig. 4*B*).

RpoS is required to adapt the cell to stationary phase and deletion of *rpoS* significantly reduced stationary phase cell density in EHEC (Fig. 4 *A*, *ii* and Fig. 4*B*). To establish if StxS acts through *rpoS* to increase stationary phase cell density, we constructed a Δ*stxS1* Δ*stxS2* Δ*rpoS* deletion strain. The triple deletion strain had a significantly reduced stationary phase cell density and complementation with *rpoS*, but not *stxS*, restored cell density to wild-type levels, indicating that StxS acts epistatically with RpoS to increase cell density in stationary phase. Collectively, these results demonstrate that StxS is required for EHEC to reach maximal stationary phase cell density under nutrient-limited conditions and that StxS activation of *rpoS* translation promotes increased cell density during stationary phase.

StxS Represses Translation of the Shiga Toxin 1B Transcript. Conflicting studies have linked RpoS regulation with Shiga toxin expression (9, 32). To determine if StxS indirectly modulates toxin expression through RpoS, wild-type EHEC and the Δ*stxS1* Δ*stxS2* double deletion strain were grown in minimal M9 media and Shiga toxin production quantified in culture supernatants by ELISA. Addition of mitomycin C induced high-level Stx expression and we found no significant difference in toxin production between the wild type and deletion strain under this condition (*SI Appendix*, Fig. S7*A*). However, in the absence of

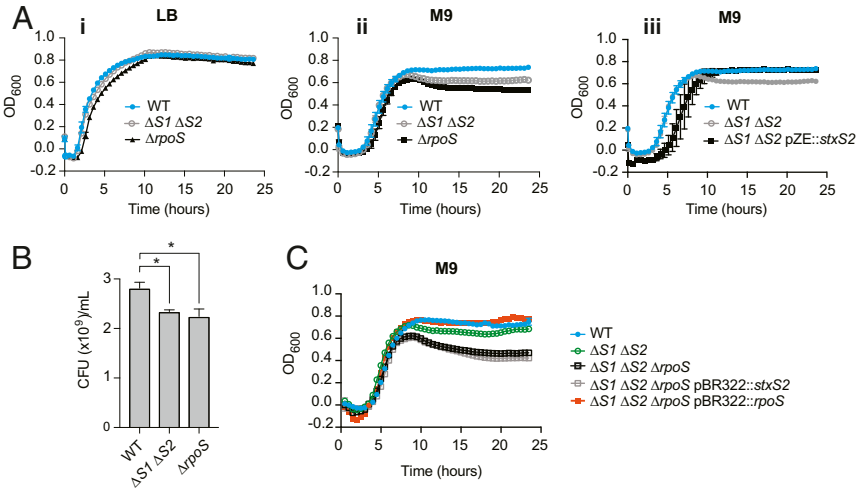

Fig. 4. StxS promotes growth to high stationary phase cell densities and requires RpoS. (*A*) Growth of EHEC (WT, filled cyan circles), Δ*stxS1*Δ*stxS2* (Δ*S1* Δ*S2*, open gray circles), and Δ*rpoS* (filled black triangles) in (*i*) rich LB media and (*ii*) minimal M9 media supplemented with glucose. (*iii*) Complementation of the Δ*stxS1* Δ*stxS2* mutant with the StxS2-expressing plasmid pZE12::*stxS* (filled black squares). Error bars represent the SD from three biological replicates. (*B*) Viable cell counts (colony forming units, CFU) of EHEC str. Sakai (WT), Δ*stxS1* Δ*stxS2*, and Δ*rpoS*. Error bars indicate SD and asterisks indicate $P > 0.05$. (*C*) Growth of EHEC (WT, filled cyan circles), Δ*stxS1* Δ*stxS2* (open green circles), Δ*stxS1* Δ*stxS2* Δ*rpoS* (open black square) in minimal M9 media supplemented with glucose. The triple deletion mutation was complemented with *stxS2* (open gray squares), or *rpoS* (filled orange squares) encoded on the medium copy number vector pBR322. Error bars represent the SD from three biological replicates.

mitomycin C, the basal level of toxin production was increased threefold in the *stxS* double deletion strain and reduced to wild-type levels in the complemented strain (Fig. 5 *A* and *B*). We had earlier established that StxS did not regulate Stxϕ propagation in rich (LB) media and we confirmed this result in nutrient-limiting conditions (M9; *SI Appendix*, Fig. S7*B*), indicating that the increased toxin yield was independent of the Stxϕ lytic switch.

Stx1 toxin is also regulated by a Fur-repressed P_{stx1} promoter and we investigated whether Stx1 or Stx2a were up-regulated in the Δ*stxS1* Δ*stxS2* mutant. RNA-seq analyses confirmed that *stx1AB*, but not *stx2AB*, is up-regulated in the double *stxS* deletion strain and restored to wild-type levels in the complemented strain (Fig. 5*C*). To determine if StxS indirectly represses Stx1 toxin expression through RpoS, we assessed toxin levels in an Δ*rpoS* background. Toxin levels were slightly elevated in the Δ*stxS1* Δ*stxS2* Δ*rpoS* triple deletion strain, and were repressed by complementation *in trans* with StxS, but not RpoS (Fig. 5*B*), indicating that StxS does not require RpoS to repress toxin expression. IntaRNA (33) was used to predict StxS binding sites within the *stx1AB* transcript and identified two potential interaction sites at positions −5 to −46 nt and +1 to −9 nt, relative to the *stx1B* start codon (Fig. 5 *D*, *Top*). These interactions were not conserved in the *stx2B* transcript. We also identified a transcription start site in our dRNA-seq data 110 nt upstream of *stx1B* with a TEX treatment enrichment factor of 2.64 (slightly below the "very specific" threshold of 3 used for our earlier analysis). Two GFP translational fusions were constructed that included the predicted StxS-*stx1B* interaction site: the first was transcribed from the upstream putative P_{stx1B} promoter, and the second included a cotranslational fusion to the last 15 codons of *stx1A* to assess repression of the bicistronic *stx1AB* transcript (*SI Appendix*, Fig. S8*A*). Both the monocistronic *stx1B* and bicistronic *stx1AB* fusions were repressed 1.88-fold and 1.65-fold respectively by StxS (Fig. 5*E*), indicating that transcripts from both P_{stx1} and putative P_{stx1B} are subject to StxS repression. Single point mutations (M1) were introduced into StxS and *stx1B* to disrupt base pairing in the longer of the two predicted StxS-*stx1B* interactions (Fig. 5 *D*, *Top*), but did not prevent StxS repression (*SI Appendix*, Fig. S8*B*). We next constructed additional point mutations (M2) to disrupt base pairing at the shorter StxS-*stx1B* interaction site positioned over the RBS and start codon (Fig. 5 *D*, *Bottom*). The M2 mutation alone did not disrupt StxS regulation; however, StxS regulation was disrupted when both M1 and M2 mutations (2M) were incorporated into *stx1B*. The *stx1B*-2M mutant was not entirely derepressed and we note that base pairing between these RNAs is not completely disrupted (*SI Appendix*, Fig. S8*D*). However, repression of *stx1B*-2M could be partly restored (22%) by providing compensatory 2M mutations in StxS (Fig. 5*F*). To further investigate the interaction between StxS and *stx1B* in vitro we used EMSA. In the presence of titrated StxS RNA, radiolabeled *stx1B* formed a slower migrating complex consistent with formation of a StxS-*stx1B* duplex (Fig. 5 *G*, *i*). This interaction was specific for *stx1B* as StxS was not able to gel shift a *stx2B* RNA fragment that is not predicted to interact (Fig. 5 *G*, *ii*). We were able to partially disrupt the StxS-*stx1B* interaction by adding an unlabeled 15mer oligonucleotide that occluded the *stx1B* M1 site. A 15mer positioned at the *stx1B* M2 site, that also partly occluded the M1 interaction, completely inhibited formation of the StxS-*stx1B* complex, as did a 48mer that occluded both M1 and M2 sites (*SI Appendix*, Fig. S9). The StxS-*stx1B* interaction was not disrupted by a 15mer positioned outside the M1 and M2 sites (*SI Appendix*, Fig. S9). These results demonstrate that StxS can directly repress *stx1B* expression and suggest that StxS interactions at both the M1 and M2 sites facilitate *stx1B* regulation. Cumulatively, our results demonstrate that StxS represses expression of Shiga toxin 1 under lysogenic conditions through direct interactions with the *stx1B* ribosomal binding site.

Discussion

Bacteriophages are important drivers of bacterial pathogenesis and evolution through horizontal transfer of DNA between hosts (1, 2). Lysogenic bacteriophage also manipulate host gene regulatory networks and modulate bacterial virulence gene expression. A stark example is commensal *E. coli* K-12 that contains nine cryptic prophage elements. Deletion of these phage remnants has a profound effect on resistance to environmental stresses, antibiotic challenge, and prevents the culture reaching high cell densities (34). Small regulatory RNAs encoded within phages have been shown to contribute to these stress tolerances.

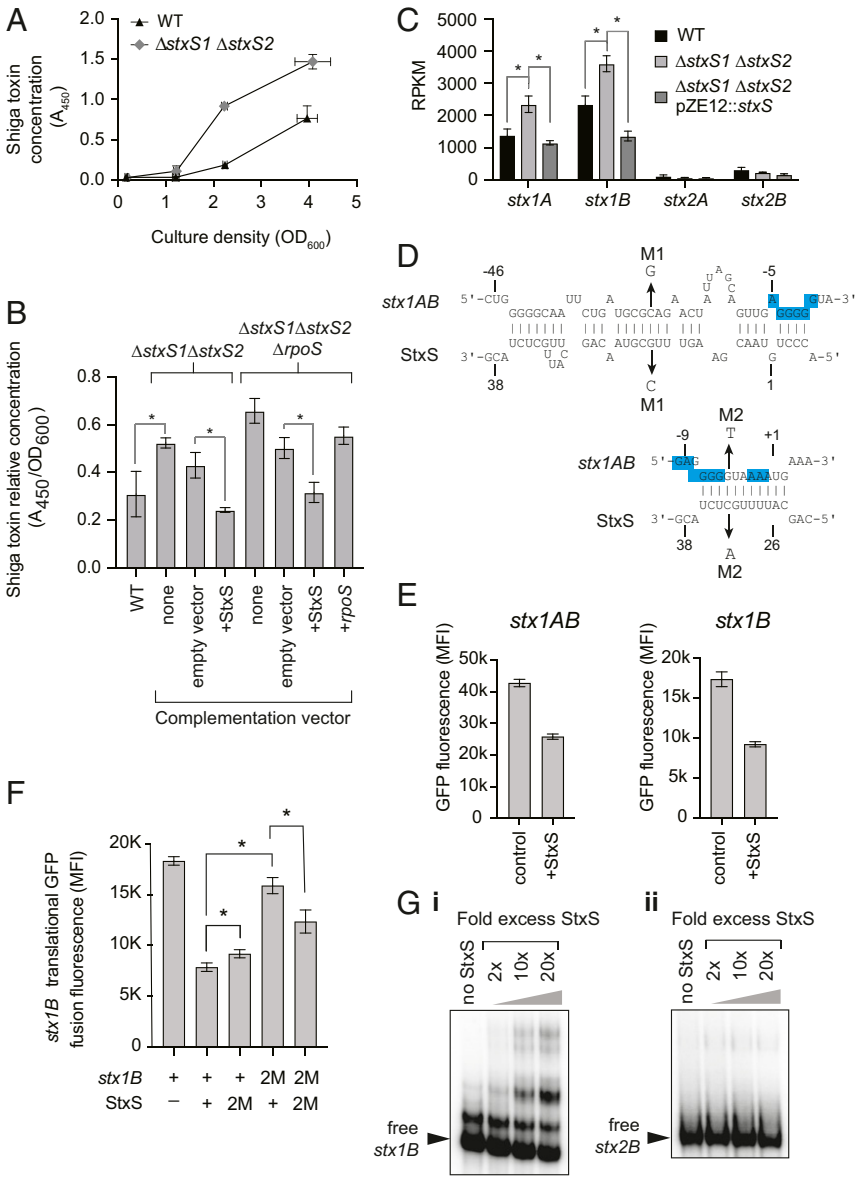

Fig. 5. The sRNA StxS represses Shiga toxin 1 expression. (*A*) Shiga toxin ELISA of EHEC (WT, triangles) and Δ*stxS1* Δ*stxS2* (circles) culture supernatants during growth in minimal M9 media. (*B*) Shiga toxin ELISA of culture supernatants from EHEC (WT), Δ*stxS1*Δ*stxS2* double deletion, and Δ*stxS1*Δ*stxS2* Δ*rpoS* triple deletion strains complemented with the empty vector (pBR322), StxS (pBR322::*stxS*), *rpoS* (pBR322::*rpoS*) or without a complementation vector (none, indicated below). (*C*) RNA-seq analysis of *stx1AB* and *stx2AB* transcript abundance in EHEC (WT), Δ*stxS1* Δ*stxS2*, and Δ*stxS1* Δ*stxS2* pZE12::*stxS* complemented strains in minimal M9 media. Error bars represent SE. Asterisks indicates a *P* value <0.05. (*D*, *Top*) Predicted base pairing between StxS and *stx1B* at site M1, and (*Bottom*) predicted interaction at site M2. The *stx1B* RBS and start codon are highlighted in blue, and M1 and M2 mutations are indicated by arrows. (*E*, *Left*) StxS repression of a cotranslational *stx1AB* fusion (pXG30SF::*stx1AB*), and (*Right*) StxS repression of a *stx1B* translational fusion (pXG10SF::*stx1B*). Control indicates a plasmid expressing a scrambled RNA sequence (pJV300). A schematic describing each fusion is presented in *SI Appendix*, Fig. S8*A*. (*F*) Compensatory point mutations demonstrate direct interaction between StxS and *stx1B* (pXG10SF::*stx1B*). Fluorescence is shown as average median fluorescence intensity and the StxS or *stx1B* allele is shown below. 2M indicates constructs that contain both M1 and M2 point mutations (*D*). Error bars represent SD. (*G*, *i*) EMSA analysis of StxS interactions with the 5′ UTR of *stx1B*. Free *stx1B* is indicated by an arrowhead and *Upper* bands indicate a slower migrating StxS-*stx1B* complex in the presence of increasing StxS. (*ii*) EMSA analysis of the negative control RNA *stx2B*. The arrowhead indicates migration of the free *stx2B* 5′ UTR.

The small RNA DicF encoded with the cryptic Qin prophage regulates cell division in *E. coli* and promotes type 3 secretion in EHEC (35–37). Cryptic prophage in EHEC also carry small RNA sponges that modulate amino acid metabolism and aerobic stress responses by inhibiting the core genome-encoded sRNAs, GcvB and FnrS (13). Here we identify a prophage-encoded sRNA that is generated by termination of the prophage late promoter $P_{R'}$ in lysogenic Shiga toxin-encoding bacteriophages. The late promoter drives transcription of the *stxAB* toxin mRNAs and processing of the prematurely terminated transcript releases a regulatory sRNA, that we term StxS. We initially identified StxS through UV cross-linking to Hfq and demonstrate that StxS is a regulatory sRNA that positively regulates RpoS, promotes growth to high cell densities under nutrient-limiting conditions, and represses Shiga toxin 1 expression during lysogeny.

The late promoter $P_{R'}$ is constitutively active in the model bacteriophage lambda (λ) and we predict that Stxϕ $P_{R'}$ is also constitutively transcribed. Northern analysis of StxS accumulation in different media and growth stages indicates that StxS is increased in stationary phase and virulence-inducing (MEM-HEPES) media.

Notably, we found that StxS transcribed from the known constitutively active promoter $P_{L\mathit{lacO\text{-}1}}$ in minimal M9 medium also accumulated in early stationary phase, indicating that the increased abundance may be due to high stability and accumulation, rather than growth stage-dependent transcriptional regulation. Stxϕ $P_{R'}$ and $t_{R'}$ are spaced 258 nt apart and we were initially surprised that the stable StxS sRNA accumulated as a 74-nt transcript. RNase E processing of the $StxS_L$ transcript generates a monophosphorylated 5′ end and cleavage may be required to stimulate $StxS_S$ activity, as has been shown for the sRNAs ArcZ and RprA (25–28), potentially through interactions with the 5′ sensing pocket of RNase E (38, 39).

$StxS_S$ uses the same seed sequence as the core genome-encoded sRNAs DsrA, ArcZ, and RprA to activate RpoS. These sRNAs have been shown to activate *rpoS* by relieving inhibitory secondary structure within the 5′ UTR of *rpoS* and by inhibiting premature Rho-dependent termination, allowing transcription of the *rpoS* CDS (29). We find that StxS is able to activate *rpoS* expression in the presence of the Rho inhibitor, BCM, and that StxS activation was additive when used in combination with BCM. Our results demonstrate that StxS can act independently of Rho, but do not preclude a Rho-dependent activity. Our full-length *rpoS*-GFP translational fusion is subject to both Rho-dependent termination and Rho-independent translational repression. The additive effects of BCM and StxS on *rpoS*-GFP expression are still consistent with dual Rho-dependent and -independent activities. Indeed, given the shared seed sequence, we predict that StxS will mimic the functions of ArcZ, DsrA, and RprA and will act through both mechanisms.

The stationary phase stress sigma factor RpoS plays a key role in regulating the virulence of many bacterial pathogens including *Salmonella* and *Vibrio* spp. In EHEC, RpoS regulates 1,135 genes in stationary phase, including the LEE encoded type 3 secretion system (31), and deletion of *rpoS* has profound effects on acid, oxidative stress, and temperature tolerance (40). RpoS is also required for colonization of cattle and survival in soil (41, 42). We found that StxS promotes a 1.7-fold increase in RpoS expression in EHEC but the Δ*stxS1* Δ*stxS2* strain was not significantly sensitive to acid and had a mild sensitivity to osmotic stress (*SI Appendix*, Fig. S6 *A–C*). We attribute this result to redundancy in RpoS-activating signals and note that the sRNA RprA activates RpoS in response to osmolarity (43), and DsrA mediates acid tolerance in EHEC (44). The StxS double deletion strain grew to a lower stationary phase cell density in minimal media, but not in rich media, and StxS accumulates under these conditions. We propose that StxS may promote growth at higher culture densities in the environment and in vivo by providing a constitutively activating signal for RpoS, at least partly uncoupling posttranscriptional regulation of *rpoS* mRNA from stress-induced signals (Fig. 6).

We have also found that the double *stxS* deletion strain produced threefold more Shiga toxin, indicating that StxS represses toxin production. This was despite no detectable difference in Stxϕ propagation between the wild and mutant strains. In EHEC strain Sakai, the Stx2aϕ is active and Stx2a toxin is transcribed from the late phage promoter $P_{R'}$ during lytic induction. The Stx1ϕ however, is cryptic and can be transcribed from both the late promoter and a Fur-regulated *stx1AB*-specific promoter (45). We have additionally identified an internal promoter (P_{stx1B}) within *stx1A* that may also drive transcription of *stx1B*. Our results suggested that in the absence of increased phage particles, the increased toxin yield in the *stxS* deletion strain was unlikely to be Stx2a. RNA-seq analysis confirmed that Stx1, but not Stx2a, is up-regulated in the *stxS* double deletion strain and repressed when complemented *in trans*. Shiga toxin levels were increased in the Δ*stxS1* Δ*stxS2* Δ*rpoS* triple deletion strain; however, we were not able to complement this phenotype *in trans* with RpoS. Our results indicate that RpoS does not regulate Stx1 production under the minimal media conditions tested here and are in line with recent work indicating that RpoS does not control Shiga toxin expression in Stx-phage lysogenized *Citrobacter rodentium* (9). Using GFP translational fusions and in vitro EMSA analysis of the StxS-*stx1B* interaction we found that StxS directly repressed *stx1B* expression through binding to the *stx1B* ribosomal binding site. IntaRNA identified potential StxS interaction sites at both the *stx1B* RBS (M2 site) and further upstream (M1 site). Point mutations in both sites (2M) were required to disrupt StxS regulation in vivo; however, both sites contributed to the StxS-*stx1B* interactions when assessed in vitro using EMSA. Compensatory 2M mutations in StxS were able to partly restore repression of the *stx1B*-2M double point mutant in vivo (−22%, Fig. 5*F*) supporting direct base pairing between these RNAs. Notably, the predicted interaction strength between the StxS-2M:*stx1B*-2M RNAs is lower (ΔG −8.38 kcal/mol, IntaRNA) (33) than the wild-type RNAs (−11.61 kcal/mol), potentially explaining the lower fold repression. Collectively, our results demonstrate that the Stx1 phage encodes an elegant regulatory circuit whereby an RNA byproduct of the antiterminated

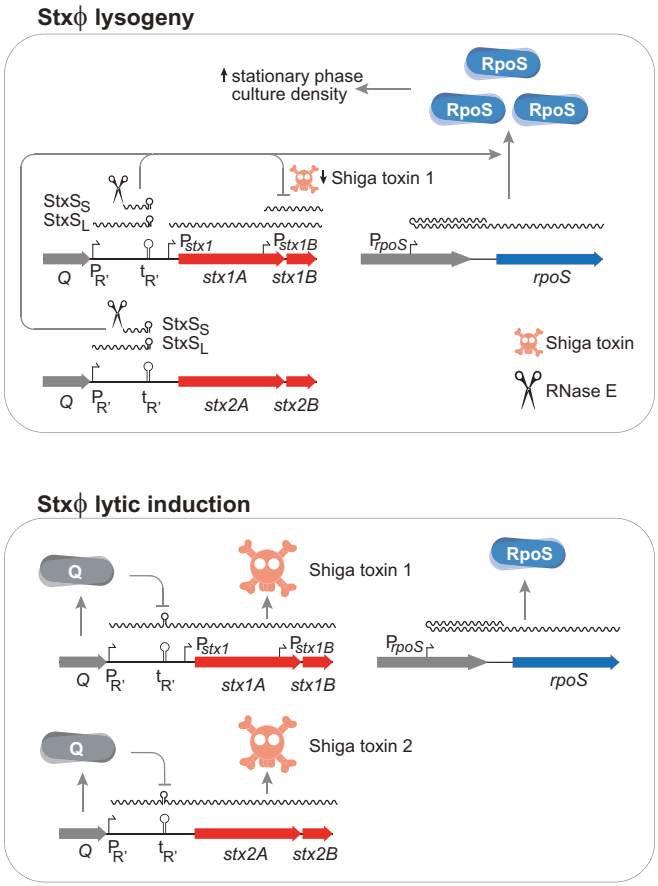

Fig. 6. Summary model of StxS sRNA function during Stx phage lysogeny and lytic induction. (*Top*) Lysogeny. The Stx1 and Stx2 phages late promoters ($P_{R'}$) are constitutively active and transcribe $StxS_L$, terminating at the intrinsic terminator $t_{R'}$. The $StxS_L$ transcript is processed by RNase E, releasing a shorter fragment termed $StxS_S$ that functions as a regulatory sRNA. During lysogeny, $StxS_S$ activates expression of the stationary phase stress response sigma factor *rpoS* (blue) and silences the expression of the Shiga toxin 1 subunit *stx1B* (red). These activities reduce Shiga toxin 1 production and increase stationary phase culture density. (*Bottom*) Lytic induction. During the lytic cycle antiterminator Q is expressed and promotes antitermination of $t_{R'}$ within both Stx phages. The constitutively active $P_{R'}$ promoter transcribes through $t_{R'}$ and into the Shiga toxin genes and downstream phage late genes including lysis genes. The $StxS_L$ sequence is incorporated into the 5′ end of the late transcript.

promoter $P_{R'}$, directly suppresses the downstream Stx1 toxin during lysogeny (summarized in Fig. 6).

Antitermination is used to regulate lytic induction in many bacteriophages and we propose that these constitutively transcribed short RNA species may provide unconstrained RNA sequence space for the selection of sRNA-like features, including chaperone binding sites and seed sequences. Given the abundance of prophage within bacterial genomes, sRNAs from antitermination-regulated promoters may represent an abundant class of regulatory sRNA. In *Salmonella* Typhimurium the cryptic Gifsy-1 phage encodes a *cis*-acting sRNA termed IsrK that is generated from an antitermination-regulated phage promoter and is required for translation of the longer antiterminated transcript (46). Interestingly, early work on the archetype bacteriophage, λ, also demonstrated that lysogens produce an abundant short transcript from the antiterminated late promoter $P_{R'}$, originally termed λ 6S RNA (47–50). Similar antitermination-regulated short RNA species are generated from the late promoters of lysogenic phages 21, ϕ80, 82, and P22 (51–54). No function has been ascribed to λ 6S RNA, although an early report speculated that it may be a noncoding RNA analogous to VA RNA of adenoviruses (47). Our work supports the idea that λ 6S RNA may function as a *trans*-acting, antiterminated noncoding RNA in this well-studied model bacteriophage and may have as yet unappreciated regulatory functions. We speculate that antitermination-regulated phage promoters may provide a rich source of unconstrained, short RNA sequences for the evolution of small RNAs.

Materials and Methods

Bacterial Growth Conditions. Bacterial strains and plasmids used for this study are listed in *SI Appendix*, Tables S3–S5. *E. coli* was routinely grown at either 30 °C or 37 °C in liquid LB, minimal M9, or MEM-HEPES supplemented with 0.1% glucose and 250 nM $Fe(NO_3)_3$, or on solid LB agar plates. Bacterial media was supplemented with ampicillin (100 μg/mL), chloramphenicol (34 μg/mL), kanamycin (50 μg/mL), spectinomycin (50 μg/mL), or tetracycline (10 μg/mL) where appropriate.

Strain Construction. Gene deletions in *E. coli* O157:H7 str. Sakai (both *stx*$^-$ and *stx*$^+$) were generated using the allelic exchange vector pTOF25 (55, 56). For deletion of *stxS1* in *E. coli* O157:H7 Sakai *stx*$^-$ and *stx*$^+$, the 5′ flanking region was amplified from genomic DNA using StxS1.DelA.SmaI.F2 (for *stx*$^-$) or StxS1.DelA.SmaI.F (for *stx*$^+$) with StxS1.DelA.NotI.R, while the 3′ flanking region was amplified using StxS1.DelB.NotI.F and StxS1.DelB.SalI.R. For deletion of *stxS2* in *E. coli* O157:H7 Sakai *stx*$^-$ and *stx*$^+$, flanking regions were amplified from genomic DNA using primer pairs StxS2.DelA.SmaI.F and StxS2.DelA.NotI.R, and StxS2.DelB.NotI.F and StxS2.DelB.SalI.R. For deletion of *rpoS* in *E. coli* O157:H7 Sakai *stx*$^-$ and *stx*$^+$, flanking regions were amplified from genomic DNA using primer pairs RpoS.DelA.SmaI.F and RpoS.DelA.NotI.R, and RpoS.DelB.NotI.F and RpoS.DelB.SalI.R. All amplified flanking regions were joined together using splicing by overlap extension (SOE) PCR. An FRT-*tetRA*-FRT cassette from pTOF1 was inserted into the allelic exchange vectors using *Not*I (55, 56). Allelic exchange was performed as per ref. 56. *tetRA* cassettes were removed from the mutants using FLP recombinase encoded on pCP20 (55, 57).

Single deletions of *stxS* in EHEC str. Sakai *stx*$^+$ (JJT384 and JJT385) were repaired using a two-plasmid CRISPR-Cas9 system (58). An sgRNA targeting the FRT scar was cloned into pTargetF using inverse PCR with primers FRT.sgRNA.F and pTARGETF.R.5P. The repair templates for *stxS1* and *stxS2* were amplified using primer pairs pTT.StxS1.F/R and pTT.StxS2.F/R, respectively. Colony PCR was used to confirm successful chromosomal repairs.

Northern Blot Analysis. Total RNA was extracted using the GTC-phenol method detailed in ref. 59. One microgram of total RNA was separated by electrophoresis on an 8% polyacrylamide TBE-urea gel, then transferred onto a nylon membrane and cross-linked in a Stratagene Auto-Crosslinker with 1,200 mJ of UV. The membranes were prehybridized for 30 min at 42 °C in Ambion ULTRAhyb Ultrasensitive hybridization buffer, then probed with 10 pmol of ^{32}P-labeled oligonucleotide for 16 h. Membranes were washed three times with 2× sodium chloride sodium phosphate EDTA (SSPE) buffer with 0.1% SDS for 15 min, then visualized using a Fuji BAS-MP 2040 phosphorscreen and imaged using a Typhoon FLA9500 (GE Healthcare).

Phylogenetic Analysis of the Q Antiterminator and StxS. Whole genome sequences for STEC isolates listed in Fig. 1*D* were downloaded from GenBank. Q antiterminators associated with either the Shiga toxins or the StxS sRNA were detected using BLAST. These sequences were extracted and aligned using MUSCLE (60). A maximum-likelihood phylogenetic tree was inferred using FastTree 2.1 (61).

Transient Inactivation of RNase E. *E. coli* str. N3431 (*rne*-3071) containing pBR322 or pBR322::*stxS2* was grown at 28 °C in LB-Amp_{100} medium to an OD_{600} of 2.0. RNase E was inactivated by shifting the incubation temperature to 44 °C for 30 min before harvesting total RNA using GTC phenol (59).

dRNA-Seq. *E. coli* O157:H7 str. Sakai *stx*$^-$ was grown to an OD_{600} of 0.8 in MEM-Hepes supplemented with 0.1% glucose and 250 nM of $Fe(NO_3)_3$. RNAProtect Bacteria reagent (Qiagen) was added to each culture before RNA was extracted using the RNeasy Mini Kit (Qiagen) according to the manufacturer's instructions. RNA samples were sequenced at Vertis Biotechnologie, and cDNA libraries were prepared as described in ref. 62. Adapter sequences were trimmed using Flexbar v3.5.0 (63) and aligned to the *E. coli* O157:H7 strain Sakai genome (accession no. NC_002695.1) using Novocraft v3.04.06. Transcription start sites were called using TSSPredator set to the "very specific" parameter (16). dRNA-seq datasets are deposited at GEO under accession GSE143631.

Term-Seq Analysis of RNA 3′ Ends. Total RNA was prepared as for dRNA-seq analysis (above) and sequenced at Vertis Biotechnologie using the Term-seq protocol described in ref. 17. Adapter sequences were trimmed using Flexbar v3.5.0 (63) and aligned to the *E. coli* O157:H7 str. Sakai genome (accession no. NC_002695.1) using Novocraft v3.04.06. Reads were mapped using scripts within the pyCRAC software package (64). Term-seq reads map to the reverse complement of RNA 3′ ends and were identified using pyGTF2sgr.py to map read start positions (–type = startpositions) mapping to antisense positions. These were filtered for positions with more than three read starts in all three replicate datasets using in-house scripts. Term-seq data are deposited at GEO under accession no. GSE14363.

RLM-RACE. The 5′ RLM-RACE was performed as previously described (13) with some modifications. Conversion of triphosphate RNA ends into monophosphates was done by mixing 6 μg of total RNA, 1 μL of 10× reaction buffer, and 1 unit of tobacco acid pyrophophatase (Epicentre, discontinued) in a 10-μL reaction and incubating at 37 °C for 1 h. A 5′ RNA linker (200 pmol) was ligated to 2 μL of the TAP-treated RNA with 1 μL of 10× T4 RNA ligase buffer, and 2 μL of T4 RNA ligase (NEB, cat no. M0204S) in a 10-μL reaction and incubated at 16 °C overnight. RNA was ethanol precipitated, and reverse transcribed to cDNA using SuperScript IV Reverse Transcriptase (Thermo Fisher, cat no. 18090010) according to the manufacturer's instructions. $StxS_S$ was amplified from cDNA using P5 and StxS.RACE.R primers. Amplicons were cloned into pGEM-T Easy (Promega, cat no. A1360) according to the manufacturer's instructions. RNA 5′ ends were identified by Sanger sequencing of at least 10 clones.

Enumeration of Shiga Toxin-Encoding Bacteriophage. Overnight cultures grown in LB broth were subcultured 1/100 into LB broth supplemented with 5 mM $CaCl_2$ or into minimal M9 medium. Where required, lysis was induced at an OD_{600} of 0.3 with 0.5 μg/mL mitomycin C and cultures were incubated for 16 h (22). Samples were centrifuged for 15 min at 4,000 × *g* and culture supernatants were filtered through a 0.22-μM low protein binding PES filter (Millex-GP). Phage were enumerated using an agar double overlay as described in ref. 23. Plates were spotted with 6 μL of phage-containing supernatant and incubated at 37 °C for 18 h.

Reporter Assays for In Vivo Verification of StxS Interactions. Interactions between StxS and *rpoS* or *stx1B* were experimentally verified using the GFP-translational fusion reporter system described in refs. 65 and 66. The 576-bp 5′ UTR of *rpoS* and the first 30 nucleotides of the coding region were amplified using RpoS.5UTR.F/R. *stx1AB* was cloned into pXG10SF or pXG30SF using the primer XG10.Stx1b.R and forward primers XG10.Stx1b.F and XG30.Stx1b.R, respectively. StxS2 was amplified from genomic DNA using StxS2.ZE12.5P.F and StxS2.ZE12.R and cloned into the pZE12-*luc* plasmid as detailed in ref. 66. Point mutants of pXG10SF::*rpoS* and pXG10SF::*stx1b* were made using the Quikchange II XL site-directed mutagenesis kit (Agilent) with the primers RpoS.T466C.F/R and Stx1b.C83G.F/R or Stx1b.A108T.F/R, respectively. Point mutants in pZE12::*stxS2* were made in the same manner using primers StxS2.A193C.F/R, StxS2.G202C.F/R, and StxS2.T216.F/R. Fluorescence

assays for sfGFP translational fusions were performed in *E. coli* str. DH5α. Overnight cultures of cotransformed *E. coli* DH5α were diluted 1/5 in 1× PBS, and fluorescence was measured using the FACSCantoII or LSRFortessa flow cytometry system (BD). Fluorescence was measured using the 530/30-nm bandpass filter. Measurements were done in biological triplicate, with 100,000 gated events taken from each sample. Median fluorescence intensity was calculated using FlowJo.

GFP transcriptional fusions of *rpoS*, *otsB*, *katE*, and *osmY* were constructed by amplifying the 5′ UTR and the first 30 nucleotides of the coding region using primer pairs pAJR.RpoS.F/R, pAJR.OtsB.F/R, pAJR.KatE.F/R, and pAJR.OsmY.F/R, respectively, and cloning into pAJR70 (67). Overnight cultures of wild type, Δ*stxS1*Δ*stxS2*, and *stxS*-complemented strains of *E. coli* O157:H7 str. Sakai *stx*$^{-}$ carrying the transcriptional fusion were subcultured 1/100 in LB media. OD_{600} and GFP fluorescence was measured at 2-h intervals for 10 h using the FLUOstar Omega microplate reader (BMG).

To investigate the role of StxS in regulating Rho termination of *rpoS*, pXG10SF::*rpoS* was cotransformed into the *E. coli* strain Top10F′ with either StxS or a scrambled sRNA control. Overnight cultures of cotransformants were subcultured 1/100 into 0.22 μm filtered LB media. Upon reaching an OD_{600} of 0.6, 200 μL of each replicate was aliquoted three times into a 96-well plate. Expression of the *rpoS*-sfGFP translational fusion and StxS sRNA were induced using 200 nM of anhydrotetracycline and 1 mM of isopropyl β-d-1-thiogalactopyranoside (IPTG), respectively. Rho activity was inhibited by adding 50 μg/mL of bicyclomycin (Santa Cruz Biotechnology, cat. no. sc-391755). OD_{600} and fluorescence readings were then taken every 15 min for 1 h.

RNA–RNA EMSA. In vitro transcription template PCR products were generated using IVT PCR primers listed in *SI Appendix*, Table S5. StxS, region 260 to 576 of the *rpoS* 5′ UTR, and the full-length 5′ UTRs of *stx1B* and *stx2B* were in vitro transcribed using T7 RNA polymerase (Roche, cat. no 10881767001) by incubating 100 ng of PCR product with 0.5 mM rNTPs, 1× transcription buffer and 40U of T7 RNA polymerase and incubating at 37 °C for 16 h. DNA template was depleted from the reactions by adding RQ1 RNase-free DNase and incubating at 37 °C for 15 min. RNA was purified using a phenol-chloroform extraction followed by ethanol precipitation and separated on an 8% polyacrylamide TBE-6M urea gel. Fragments corresponding to full-length transcripts were cut out, crushed, and incubated at 4 °C for 16 h in 500 μL RNA gel elution buffer (10 mM magnesium acetate, 0.5 M ammonium acetate, 1 mM ethylene diamine tetraacetic acid [EDTA]). Elution buffer was separated from crushed gel pieces by centrifugation, and RNA was extracted using phenol-chloroform and ethanol precipitation. Approximately 25 pmol of RNA was dephosphorylated using Quick CIP (New England Biolabs, cat no. M0525S) followed by another round of phenol-chloroform extraction and ethanol precipitation. RNA was radiolabeled with γ^{32}P using T4 polynucleotide kinase. Excess nucleotides were removed using a MicroSpin G-50 column (Cytiva, cat no. 27533001), and RNA was gel purified as described above.

To analyze StxS binding with the 5′ UTRs of *stx1B*, *stx2B*, and *rpoS*, ∼50 fmol of each radiolabeled mRNA was incubated with 100, 500, and 1,000 fmol of StxS in 1× duplex buffer (40 mM Tris-acetate, 0.5 mM magnesium acetate, 100 mM NaCl) in a 10 μL reaction. Reactions were first heated to 95 °C for 5 min, then incubated for 2 h at 37 °C. Samples were run on a 6% polyacrylamide 0.5× TBE + 5% glycerol gel at 16 V/cm (or 1.33 mA/cm) for 3 h before drying and visualization using a Fuji BAS-MP 2040 phosphorscreen and Typhoon FLA9500 (GE Healthcare).

To confirm StxS binding sites on *stx1B*, ∼50 fmol of radiolabeled *stx1B* was incubated with 2.5 pmol of oligonucleotides antisense to different regions of the *stx1B* 5′ UTR in the presence or absence of 1 pmol of StxS. Reactions were annealed and run on a 6% polyacrylamide 0.5× TBE + 5% glycerol gel as previously described.

Growth Curve Measurements. The growth curves of *E. coli* O157:H7 str. Sakai *stx*$^{-}$ in various nutrient conditions were measured using the Bioscreen C MBR (Growth Curves USA). The OD_{600} of overnight LB broth cultures was first normalized and then diluted 1/100 into 300 μL of growth media in a Bioscreen Honeycomb 100-well plate (Thermo Fisher, cat no. 9502550). The plate was incubated in the Bioscreen C at 37 °C with continuous low shaking. OD_{600} readings were taken every 20 min for 24 h. Growth experiments were performed at least twice, and representative data are presented. Error bars represent SE of triplicate cultures.

Measurement of Stx Production in EHEC. Overnight cultures of wild-type, mutant, and complemented strains of EHEC str. Sakai *stx*$^{+}$ in LB broth were washed and subcultured 1/100 into minimal M9 medium. Samples were collected after 4, 6, 8, and 10 h and centrifuged at 16,000 × *g* for 1 min. Culture supernatants were diluted 1/50 in minimal M9 medium and used in a RIDASCREEN Verotoxin (R-Biopharm) ELISA (C2201) according to the manufacturer's instructions.

RNA Sequencing and Analysis. Total RNA was harvested from triplicate samples of wild type, Δ*stxS1* Δ*stxS2*, and complemented strains of *E. coli* O157:H7 str. Sakai *stx*$^{+}$ using GTC phenol extraction. Genomic DNA was removed using RQ1 RNase-free DNase (Promega), and RNA was repurified using a phenol-chloroform extraction. Samples were submitted to the Ramaciotti Centre for Genomics for single-end sequencing on the NextSeq500 (Illumina) platform. RNA-seq data are deposited at GEO under accession GSE14363.

Differential expression analysis of sequencing reads was performed using the READemption pipeline (v 0.5.0) (68).

Data Availability. Sequencing datasets generated in this study are available at NCBI GEO under the accession number GSE14363. Previously published Hfq binding data are available at NCBI GEO under BioProject number PRJNA197291. RNase E binding data and CLASH sRNA interaction data are available under PRJNA310426. dRNA-seq datasets are deposited at GEO under accession GSE143631.

ACKNOWLEDGMENTS. We would like to acknowledge technical support from Dr. Michael Payne. B.M.S. was supported by a Research Training Program Scholarship from the Australian Government. J.J.T. and B.M.S. were supported by funding from the National Health and Medical Research Council (GNT1161161). Flow cytometry in this work was performed at the Mark Wainwright Analytical Centre of the University of New South Wales (UNSW) Sydney, which is part funded by the Research Infrastructure Programme of UNSW Sydney.

1. E. F. Boyd, Bacteriophage-encoded bacterial virulence factors and phage-pathogenicity island interactions. *Adv. Virus Res.* **82**, 91–118 (2012).
2. H. Brüssow, C. Canchaya, W.-D. Hardt, Phages and the evolution of bacterial pathogens: From genomic rearrangements to lysogenic conversion. *Microbiol. Mol. Biol. Rev.* **68**, 560–602 (2004).
3. A. R. Melton-Celsa, Shiga toxin (Stx) classification, structure, and function. *Microbiol. Spectr.* **2**, EHEC-0024-2013 (2014).
4. T. K. Davis, N. C. A. J. Van De Kar, P. I. Tarr, Shiga toxin/verocytotoxin-producing Escherichia coli infections: Practical clinical perspectives. *Microbiol Spectr.* **2**, EHEC-0025-2014 (2014).
5. Centers for Disease Control and Prevention, *National Enteric Disease Surveillance: Shiga toxin-producing Escherichia coli (STEC) Annual Report, 2013*, (US Department of Health and Human Services, Atlanta, GA, 2016).
6. D. J. Ingle *et al.*, Emergence and divergence of major lineages of Shiga-toxin-producing Escherichia coli in Australia. *Microb. Genomics.* **5**, e000268 (2019).
7. P. L. Wagner *et al.*, Role for a phage promoter in Shiga toxin 2 expression from a pathogenic *Escherichia coli* strain. *J. Bacteriol.* **183**, 2081–2085 (2001).
8. P. L. Wagner *et al.*, Bacteriophage control of Shiga toxin 1 production and release by *Escherichia coli*. *Mol. Microbiol.* **44**, 957–970 (2002).
9. S. Balasubramanian, M. S. Osburne, H. BrinJones, A. K. Tai, J. M. Leong, Prophage induction, but not production of phage particles, is required for lethal disease in a microbiome-replete murine model of enterohemorrhagic *E. coli* infection. *PLoS Pathog.* **15**, 1–27 (2019).
10. S. R. Casjens, R. W. Hendrix, Bacteriophage lambda: Early pioneer and still relevant. *Virology* **479–480**, 310–330 (2015).
11. S. B. Calderwood, J. J. Mekalanos, Iron regulation of Shiga-like toxin expression in Escherichia coli is mediated by the Fur locus. *J. Bacteriol.* **169**, 4759–4764 (1987).
12. K. Ichimura *et al.*, Nitric oxide-enhanced Shiga toxin production was regulated by Fur and RecA in enterohemorrhagic *Escherichia coli* O157. *MicrobiologyOpen* **6**, 1–17 (2017).
13. J. J. Tree, S. Granneman, S. P. McAteer, D. Tollervey, D. L. Gally, Identification of bacteriophage-encoded anti-sRNAs in pathogenic *Escherichia coli*. *Mol. Cell* **55**, 199–213 (2014).
14. S. Dahan *et al.*, Transcriptome of enterohemorrhagic *Escherichia coli* O157 adhering to eukaryotic plasma membranes. *Infect. Immun.* **72**, 5452–5459 (2004).
15. Y. Ogura *et al.*, The Shiga toxin 2 production level in enterohemorrhagic *Escherichia coli* O157:H7 is correlated with the subtypes of toxin-encoding phage. *Sci. Rep.* **5**, 16663 (2015).
16. G. Dugar *et al.*, High-resolution transcriptome maps reveal strain-specific regulatory features of multiple *Campylobacter jejuni* isolates. *PLoS Genet.* **9**, e1003495 (2013).
17. D. Dar *et al.*, Term-seq reveals abundant ribo-regulation of antibiotics resistance in bacteria. *Science* **352**, aad9822 (2016).
18. S. A. Waters *et al.*, Small RNA interactome of pathogenic *E. coli* revealed through crosslinking of RNase E. *EMBO J.* **36**, 374–387 (2017).
19. Y. Chao *et al.*, In vivo cleavage map illuminates the central role of RNase E in coding and noncoding RNA pathways. *Mol. Cell* **65**, 39–51 (2017).
20. I. B. Dodd, K. E. Shearwin, J. B. Egan, Revisited gene regulation in bacteriophage λ. *Curr. Opin. Genet. Dev.* **15**, 145–152 (2005).

21. L. Krinke, M. Mahoney, D. L. Wulff, The role of the OOP antisense RNA in coliphage λ development. *Mol. Microbiol.* **5**, 1265–1272 (1991).
22. L. Bonanno, M.-A. Petit, E. Loukiadis, V. Michel, F. Auvray, Heterogeneity in induction level, infection ability, and morphology of Shiga toxin-encoding phages (Stx phages) from dairy and human Shiga toxin-producing *Escherichia coli* O26:H11 isolates. *Appl. Environ. Microbiol.* **82**, 2177–2186 (2016).
23. M. R. Islam *et al*., A sensitive and simple plaque formation method for the Stx2 phage of *Escherichia coli* O157:H7, which does not form plaques in the standard plating procedure. *Plasmid* **67**, 227–235 (2012).
24. N. R. Markham, M. Zuker, UNAFold: Software for nucleic acid folding and hybridization. *Methods Mol. Biol.* **453**, 3–31 (2008).
25. T. Soper, P. Mandin, N. Majdalani, S. Gottesman, S. A. Woodson, Positive regulation by small RNAs and the role of Hfq. *Proc. Natl. Acad. Sci. U.S.A.* **107**, 9602–9607 (2010).
26. R. A. Lease, M. E. Cusick, M. Belfort, Riboregulation in *Escherichia coli*: DsrA RNA acts by RNA:RNA interactions at multiple loci. *Proc. Natl. Acad. Sci. U.S.A.* **95**, 12456–12461 (1998).
27. N. Majdalani, D. Hernandez, S. Gottesman, Regulation and mode of action of the second small RNA activator of RpoS translation, RprA. *Mol. Microbiol.* **46**, 813–826 (2002).
28. N. Majdalani, C. Cunning, D. Sledjeski, T. Elliott, S. Gottesman, DsrA RNA regulates translation of RpoS message by an anti-antisense mechanism, independent of its action as an antisilencer of transcription. *Proc. Natl. Acad. Sci. U.S.A.* **95**, 12462–12467 (1998).
29. N. Sedlyarova *et al*., sRNA-mediated control of transcription termination in *E. coli*. *Cell* **167**, 111–121.e13 (2016).
30. Y. Peng, T. J. Soper, S. A. Woodson, Positional effects of AAN motifs in *rpoS* regulation by sRNAs and Hfq. *J. Mol. Biol.* **426**, 275–285 (2014).
31. T. Dong, H. E. Schellhorn, Global effect of RpoS on gene expression in pathogenic *Escherichia coli* O157:H7 strain EDL933. *BMC Genomics* **10**, 349 (2009).
32. L. Imamovic, E. Ballesté, A. Martínez-Castillo, C. García-Aljaro, M. Muniesa, Heterogeneity in phage induction enables the survival of the lysogenic population. *Environ. Microbiol.* **18**, 957–969 (2016).
33. M. Mann, P. R. Wright, R. Backofen, IntaRNA 2.0: Enhanced and customizable prediction of RNA-RNA interactions. *Nucleic Acids Res.* **45**, W435–W439 (2017).
34. X. Wang *et al*., Cryptic prophages help bacteria cope with adverse environments. *Nat. Commun.* **1**, 147–149 (2010).
35. D. Balasubramanian, P. T. Ragunathan, J. Fei, C. K. Vanderpool, A prophage-encoded small RNA controls metabolism and cell division in *Escherichia coli*. *mSystems* **1**, e00021-15 (2016).
36. F. Tétart, J.-P. Bouché, Regulation of the expression of the cell-cycle gene *ftsZ* by DicF antisense RNA. Division does not require a fixed number of FtsZ molecules. *Mol. Microbiol.* **6**, 615–620 (1992).
37. E. M. Melson, M. M. Kendall, The sRNA DicF integrates oxygen sensing to enhance enterohemorrhagic *Escherichia coli* virulence via distinctive RNA control mechanisms. *Proc. Natl. Acad. Sci. U.S.A.* **116**, 14210–14215 (2019).
38. A. J. Callaghan *et al*., Structure of Escherichia coli RNase E catalytic domain and implications for RNA turnover. *Nature* **437**, 1187–1191 (2005).
39. S. M. Garrey *et al*., Substrate binding and active site residues in RNases E and G: Role of the 5′-sensor. *J. Biol. Chem.* **284**, 31843–31850 (2009).
40. S. Gottesman, Trouble is coming: Signaling pathways that regulate general stress responses in bacteria. *J. Biol. Chem.* **294**, 11685–11700 (2019).
41. S. B. Price *et al*., Role of *rpoS* in acid resistance and fecal shedding of *Escherichia coli* O157:H7. *Appl. Environ. Microbiol.* **66**, 632–637 (2000).
42. A. H. A. M. van Hoek, H. J. M. Aarts, E. Bouw, W. M. van Overbeek, E. Franz, The role of *rpoS* in *Escherichia coli* O157 manure-amended soil survival and distribution of allelic variations among bovine, food and clinical isolates. *FEMS Microbiol. Lett.* **338**, 18–23 (2013).
43. R. Madhugiri, S. R. Basineni, G. Klug, Turn-over of the small non-coding RNA RprA in *E. coli* is influenced by osmolarity. *Mol. Genet. Genomics* **284**, 307–318 (2010).
44. R. A. Lease, D. Smith, K. McDonough, M. Belfort, The small noncoding DsrA RNA is an acid resistance regulator in *Escherichia coli*. *J. Bacteriol.* **186**, 6179–6185 (2004).
45. M. Asadulghani *et al*., The defective prophage pool of *Escherichia coli* O157: Prophage-prophage interactions potentiate horizontal transfer of virulence determinants. *PLoS Pathog.* **5**, e1000408 (2009).
46. T. Hershko-Shalev *et al*., Gifsy-1 prophage IsrK with dual function as small and messenger RNA modulates vital bacterial machineries. *PLoS Genet.* **12**, e1005975 (2016).
47. P. Lebowitz, S. M. Weissman, C. M. Radding, Nucleotide sequence of a ribonucleic acid transcribed in vitro from lambda phage deoxyribonucleic acid. *J. Biol. Chem.* **246**, 5120–5139 (1971).
48. J. Sklar, P. Yot, S. M. Weissman, Determination of genes, restriction sites, and DNA sequences surrounding the 6S RNA template of bacteriophage lambda. *Proc. Natl. Acad. Sci. U.S.A.* **72**, 1817–1821 (1975).
49. D. L. Daniels, M. N. Subbarao, F. R. Blattner, H. A. Lozeron, Q-mediated late gene transcription of bacteriophage λ: RNA start point and RNase III processing sites *in vivo*. *Virology* **167**, 568–577 (1988).
50. J. L. Sklar, *Structure and Function of Two Regions of DNA Controlling the Synthesis of Prokaryotic RNAs*, (Yale University, New Haven, CT, 1977).
51. M. G. Schechtman, J. D. Snedeker, J. W. Roberts, Genetics and structure of the late gene regulatory region of phage 82. *Virology* **105**, 393–404 (1980).
52. J. W. Roberts, Transcription termination and late control in phage lambda. *Proc. Natl. Acad. Sci. U.S.A.* **72**, 3300–3304 (1975).
53. H. C. Guo, M. Kainz, J. W. Roberts, Characterization of the late-gene regulatory region of phage 21. *J. Bacteriol.* **173**, 1554–1560 (1991).
54. J. W. Roberts, C. W. Roberts, S. Hilliker, D. Botstein, "Transcription termination and regulation in bacteriophages P22 and lambda" in *RNA Polymerase*, R. Losick, M. Chamberlain, Eds. (Cold Spring Harbor Laboratory Press, Cold Spring Harbor, NY, 1976), pp. 707–718.
55. C. Merlin, S. McAteer, M. Masters, Tools for characterization of *Escherichia coli* genes of unknown function. *J. Bacteriol.* **184**, 4573–4581 (2002).
56. J. J. Tree *et al*., Transcriptional regulators of the GAD acid stress island are carried by effector protein-encoding prophages and indirectly control type III secretion in enterohemorrhagic Escherichia coli O157:H7. *Mol. Microbiol.* **80**, 1349–1365 (2011).
57. P. P. Cherepanov, W. Wackernagel, Gene disruption in *Escherichia coli*: TcR and KmR cassettes with the option of Flp-catalyzed excision of the antibiotic-resistance determinant. *Gene* **158**, 9–14 (1995).
58. Y. Jiang *et al*., Multigene editing in the *Escherichia coli* genome via the CRISPR-Cas9 system. *Appl. Environ. Microbiol.* **81**, 2506–2514 (2015).
59. D. Tollervey, I. W. Mattaj, Fungal small nuclear ribonucleoproteins share properties with plant and vertebrate U-snRNPs. *EMBO J.* **6**, 469–476 (1987).
60. R. C. Edgar, MUSCLE: Multiple sequence alignment with high accuracy and high throughput. *Nucleic Acids Res.* **32**, 1792–1797 (2004).
61. M. N. Price, P. S. Dehal, A. P. Arkin, FastTree 2–Approximately maximum-likelihood trees for large alignments. *PLoS One* **5**, e9490 (2010).
62. C. M. Sharma *et al*., The primary transcriptome of the major human pathogen *Helicobacter pylori*. *Nature* **464**, 250–255 (2010).
63. M. Dodt, J. T. Roehr, R. Ahmed, C. Dieterich, FLEXBAR—Flexible barcode and adapter processing for next-generation sequencing platforms. *Biology (Basel)* **1**, 895–905 (2012).
64. S. Webb, R. D. Hector, G. Kudla, S. Granneman, PAR-CLIP data indicate that Nrd1-Nab3-dependent transcription termination regulates expression of hundreds of protein coding genes in yeast. *Genome Biol.* **15**, R8 (2014).
65. C. P. Corcoran *et al*., Superfolder GFP reporters validate diverse new mRNA targets of the classic porin regulator, MicF RNA. *Mol. Microbiol.* **84**, 428–445 (2012).
66. J. H. Urban, J. Vogel, Translational control and target recognition by *Escherichia coli* small RNAs in vivo. *Nucleic Acids Res.* **35**, 1018–1037 (2007).
67. A. J. Roe *et al*., Heterogeneous surface expression of EspA translocon filaments by *Escherichia coli* O157:H7 is controlled at the posttranscriptional level. *Infect. Immun.* **71**, 5900–5909 (2003).
68. K. U. Förstner, J. Vogel, C. M. Sharma, READemption-a tool for the computational analysis of deep-sequencing-based transcriptome data. *Bioinformatics* **30**, 3421–3423 (2014).